Article:
Edelmann, Daniel B, Jakob, Anna M, Wilson, Laurence G et al. (2025) Role of a single MCP in evolutionary adaptation of Shewanella putrefaciens for swimming in planktonic and structured environments. Applied and Environmental Microbiology. e0022925. ISSN: 0099-2240

https://doi.org/10.1128/aem.00229-25

AMERICAN SOCIETY FOR MICROBIOLOGY | Applied and Environmental Microbiology

| Bacteriology | Full-Length Text

Role of a single MCP in evolutionary adaptation of *Shewanella putrefaciens* for swimming in planktonic and structured environments

Daniel B. Edelmann,[1] Anna M. Jakob,[1] Laurence G. Wilson,[2] Rémy Colin,[3] David Brandt,[4] Frederik Eck,[1] Jörn Kalinowski,[4] Kai M. Thormann[1]

AUTHOR AFFILIATIONS See affiliation list on p. 16.

ABSTRACT Bacteria can adapt to their environments by changing phenotypic traits by mutations. However, improving one trait often results in the deterioration of another one, a trade-off that limits the degree of adaptation. The gammaproteobacterium *Shewanella putrefaciens* CN-32 has an elaborate motility machinery comprising two distinct flagellar systems and an extensive chemotaxis array with 36 methyl-accepting chemotaxis sensor proteins (MCPs). In this study, we performed experimental selection on S. *putrefaciens* for increased spreading through a porous environment. We readily obtained a mutant that showed a pronounced increase in covered distance. This phenotype was almost completely caused by a deletion of 24 bp from the chromosome, which leads to a moderately enhanced production of a single MCP. Accordingly, chemotaxis assays under free-swimming conditions and cell tracking in soft agar showed that the mutation improved navigation through nutritional gradients. In contrast, further increased levels of the MCP negatively affected spreading. The study demonstrates how moderate differences in the abundance of a single MCP can lead to an efficient upgrade of chemotaxis in specific environments at a low expense of cellular resources.

IMPORTANCE Experimental evolution experiments have been used to determine the trade-offs occurring in specific environments. Several studies that have used the spreading behavior of bacteria in structured environments identified regulatory mutants that increase the swimming speed of the cells. While this results in a higher chemotaxis drift, the growth fitness decreases as the higher swimming speed requires substantial cellular resources. Here we show that rapid chemotaxis adaptation can also be achieved by modifying the chemotaxis signal input at a low metabolic cost for the cell.

KEYWORDS evolution, flagellar motility, chemotaxis, flagellar system, MCP, signal perception

Many bacteria are motile by means of flagella, which are long helical proteinaceous filaments that extend from the cell surface and are rotated by a cell envelope-embedded motor. Flagella allow swimming through liquid environments and swarming across appropriate surfaces (1–3). To allow navigation toward or away from certain environmental conditions and to get access to nutrients, bacterial flagellar motility is controlled by one or more chemotaxis systems (4). Environmental signals are perceived by different methyl-accepting chemotaxis sensor proteins (MCPs), which assemble into large arrays within the cytoplasmic membrane. The signals sensed by the MCPs affect the activity of the chemotaxis histidine kinase CheA, which phosphorylates the response regulator CheY. CheY ~*P* directly interacts with the flagellar motor(s) to induce switches in the rotational direction or, in some cases, pausing of rotation, which change the

Editor Pablo Ivan Nikel, Danmarks Tekniske Universitet The Novo Nordisk Foundation Center for Biosustainability, Kgs. Lyngby, Denmark

Address correspondence to Kai M. Thormann, kai.thormann@mikro.bio.uni-giessen.de.

The authors declare no conflict of interest.

See the funding table on p. 16.

Received 28 January 2025
Accepted 21 February 2025
Published 25 March 2025

direction of movement by various mechanisms. By adjusting the run lengths between reorientation events according to the cues sensed by the MCPs, the cells modulate their otherwise random walk and can thus actively move up or down a gradient of these cues (5–8).

The formation and operation of one or more flagella is metabolically costly and results in a significant growth disadvantage of flagellated cells under uniform culturing conditions, where motility does not provide an advantage (9–12). Therefore, the regulation of motility gene expression has evolved in a way to optimize the fitness trade-off between the metabolic burden and the benefit of chemotaxis and motility in dependence on the corresponding environmental conditions (13–18). Accordingly, an elaborate gene network regulates the expression and formation of bacterial flagella and chemotaxis systems as a function of environmental cues (19–22). A well-studied system for such a regulation is the carbon catabolite repression of *Escherichia coli*, which shows that flagella-mediated motility and chemotaxis become more important in environments where carbon sources are scarce (17, 19, 23–25). Thus, *E. coli* follows a growth strategy when carbon sources are plentiful but switches to a search strategy when the carbon source is scarce (17, 18).

Experimental evolution approaches on bacteria with respect to enhanced chemotaxis have shown that the balance between growth and motility can be readily shifted by mutations. In the cases that have been studied in more detail, enhanced chemotaxis could be mainly attributed to an elevated expression of flagellar genes, which resulted in a higher swimming speed and, by this, an increased chemotactic drift (14, 16, 18).

Shewanella putrefaciens CN-32 is a facultatively anaerobic gammaproteobacterium. Compared to *E. coli*, which harbors peritrichous flagella and a single chemotaxis system with five MCPs, the flagella and chemotaxis machinery of this species is considerably more intricate. *S. putrefaciens* possesses two distinct flagellar systems, a polar and a lateral system, which are encoded in two separate gene clusters (26). In this species, the monopolar flagellum is the primary system that is formed under most conditions and mediates main propulsion, screw thread motility, and chemotactic responses (26, 27). The chemotaxis system is located at the flagellated cell pole (28) and has an extensive signal perception range with 36 putative methyl-accepting chemotaxis sensor proteins (MCPs). The secondary flagellar cluster of *S. putrefaciens* leads to the formation of one to five lateral flagella, whose motors do not respond to the chemotactic system. As also seen in other species, such as *Vibrio alginolyticus*, they are unidirectional and solely turn counterclockwise (29, 30), and, in contrast to the paradigmatic *E. coli* flagellar system, they do not form a bundle driving propulsion (31). The additional flagella provide benefits when moving through structured environments and lower the turning angles during directional switches of the cells during chemotaxis. By this, they positively affect spreading in structured and liquid environments (30, 31). Their formation is induced in a subpopulation of cells when complex nutrients are available and likely under conditions of high load on the main polar flagella. However, the regulatory mechanisms underlying the formation of the lateral flagella system are still mostly obscure (32).

Previous studies have demonstrated that *S. putrefaciens* efficient motility and spreading in structured environments such as soft agar depend on numerous factors. These include the nutrient content of the medium, the cells' chemotactic ability, the geometry of the polar filament, and the presence of lateral flagella. In addition, the c-di-GMP-dependent production of adhesion factors, such as the mannose-sensitive hemagglutinin (MSHA) type 4 pili, influences spreading (26, 27, 30, 31, 33–35). Considering the more intricate flagellar set-up of *S. putrefaciens* as compared to that of *E. coli*, we asked whether an experimental evolution toward better spreading would yield regulatory mutants affecting the polar and/or lateral flagellar system. To answer this question, we evolved mutants with enhanced spreading capability in soft agar. Instead of differences in global regulation of flagellation, we identified a mutation that leads to a slightly increased production of a single MCP and the resulting increased chemotaxis in the selection environment as the almost exclusive reason for the observed pronounced

increase in spreading. Thus, rapid chemotaxis adaptation can be achieved through a modification of chemotaxis signal perception at a low metabolic cost for the cell.

RESULTS

S. putrefaciens soft-agar spreading evolution

A number of different factors can affect *S. putrefaciens* spreading in structured porous environments. To get more insights into the importance and regulation of the different factors, e.g., the regulation of the secondary lateral flagellar system, we adopted an experimental evolution approach. We aimed at isolating spontaneous mutants of *S. putrefaciens* that are better able to spread through soft agar, a common assay to determine the motility and the chemotaxis ability of bacteria. To monitor easily via fluorescence microscopy the flagellation status, a possible target of our selection pressure, we used for the spreading evolution approach an *S. putrefaciens* CN-32 strain that allows coupling of maleimide-ligated fluorescent dyes to both the polar and lateral filaments. For dye coupling, the flagellin-encoding genes were mutated for the flagellins to harbor serine-to-cysteine substitutions at surface-exposed positions on the flagellar filament (31). Within this study, this strain will be referred to as wild type.

The procedure of the experimental evolution is depicted in Fig. 1A. Cells from an exponentially growing culture were spotted on an LB soft-agar plate and were allowed to spread for 24 h. Cells were then isolated from the fringes of the visible spreading zones and re-inoculated on fresh LB soft agar. After 14 repetitions, the isolated cells exhibited a highly increased spreading diameter (Fig. 1B and C). The enhanced spreading phenotype was stably retained after taking the strain into stock and culturing on solid or liquid media. Thus, we considered the mutation genetically fixed. The mutant strain was referred to as *S. putrefaciens* G14.

Time-lapse scans show that the evolved strain G14 instantly outperforms the wild type in spreading and constantly outpaces the wild type as spreading zones grow (see Movie S1). Therefore, we assumed that the advantage in soft-agar motility is present at inoculation and does not develop at a later stage of spreading.

Enhanced spreading mutant cells are not affected in flagellation and morphology

Previous studies showed that the production of lateral flagella and the length of the main polar filament affect the spreading of *S. putrefaciens* in soft agar (27, 30, 33). As the next step, we therefore determined the flagellation state of wild-type and G14-mutant cells. To this end, cells were isolated from planktonic cultures and soft-agar plates. The flagellar filaments were fluorescently labeled and then used for microscopic observation. The cell morphology did not differ between mutant and wild-type cells, and we observed no significant difference in the main filament length (Fig. 2; Fig. S1). The number of flagellated cells remained similar, as did the average flagellar number per cell. Previous studies showed that, during spreading through soft agar, the polar flagellar system of *S. putrefaciens* provides main propulsion and is required for chemotactic responses. The lateral flagella provide additional propulsion and may alter the cell's turning angles during chemotactic directional switches. *S. putrefaciens* mutant cells with lateral flagella only exhibit a pronounced decrease in spreading (30). Thus, we conclude that the flagellar number in the obtained mutant is not shifted toward lateral filaments and that mutations affecting the general regulation of flagellation are unlikely.

Identification of a single MCP as the main cause of increased spreading

To identify the nature of the mutation underlying the increase in spreading, three different clones of the evolved up-motile strain G14 were sequenced and analyzed for mutations potentially affecting motility (see File S1). Apart from the cysteine substitutions in the flagellins, the only directly flagella-regulated mutation occurring in all sequenced mutants was a deletion of 24 bp upstream of the orphan gene

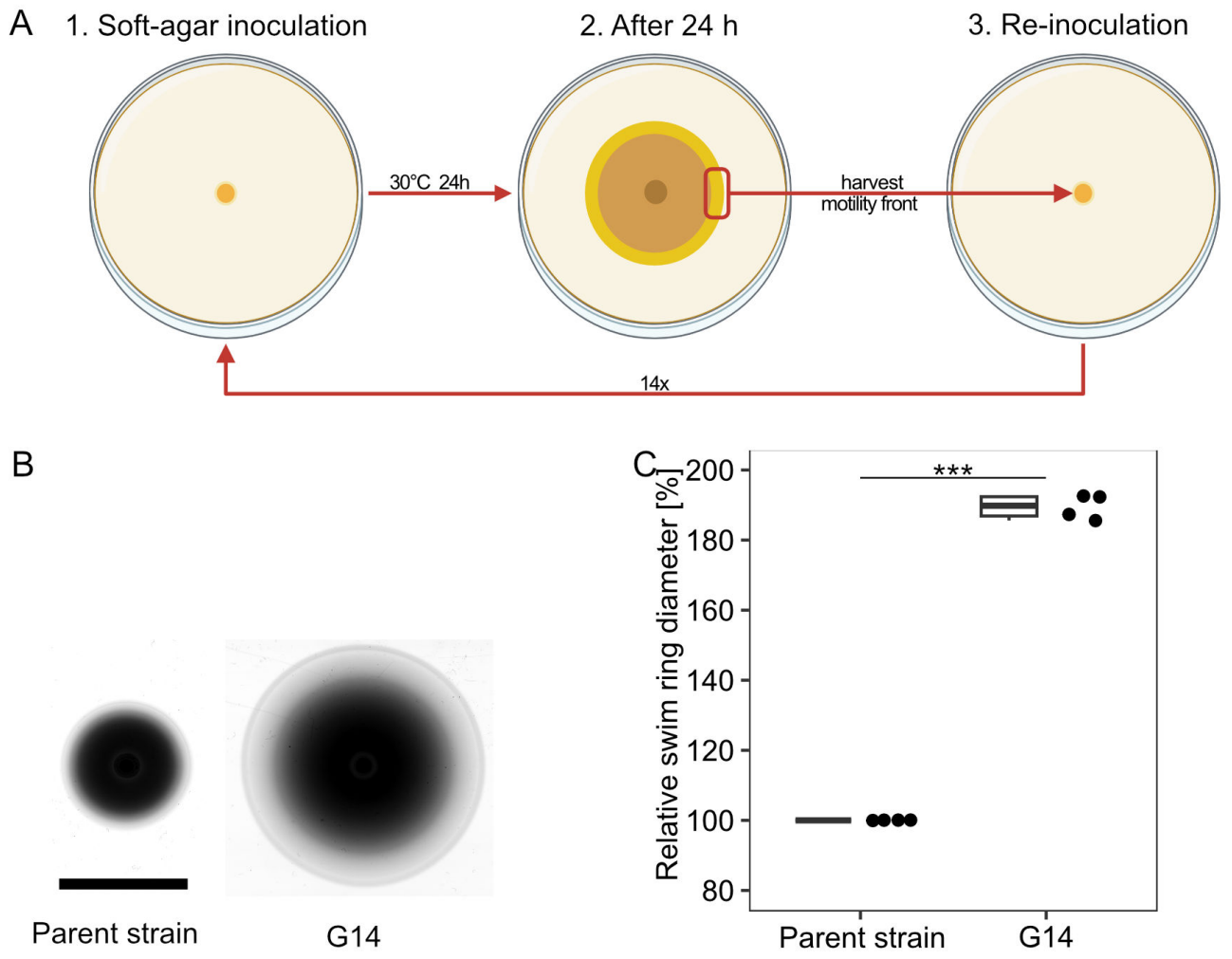

FIG 1 Isolation of an *S. putrefaciens* CN-32 spreading mutant by experimental evolution. (A) Procedure of isolation. An *S. putrefaciens* strain was allowed to spread on LB soft agar for 24 h. Cell material was isolated from the outer fringes of the spreading zone and re-inoculated on soft agar. The procedure was repeated 14 times. (B) Comparison of the parent and the evolved strain (G14) on soft agar. (C) Quantification of the spreading radius of four independent experiments. The asterisks indicate the significance according to a pairwise.t.test ($P < 0.001$).

Sputcn32_0387 (Fig. 3A). The predicted encoded protein is 638 amino acids in length, has a molecular mass of 69 kDa, and represents one of the 36 MCPs encoded by *S. putrefaciens* CN-32. The N-terminal region (up to amino acid position 287) of the MCP (from now on referred to as MCP_0387) is predicted to localize to the periplasm and possesses a Cache_3-Cache_2 domain, which likely serves in signal perception. The identity of the signal is currently unknown. Homology comparisons indicate that homologous MCPs are present in numerous other species of *Shewanella*. As the deletion upstream of MCP_0387 was the only mutation that was apparently directly related to flagella-mediated motility, we focused on the role of this mutation in the enhanced spreading phenotype.

The deleted region is located 37 bp upstream of the MCP-encoding gene's start codon. To first determine whether MCP_0387 is involved in enhanced spreading through soft agar, we introduced an in-frame deletion of the corresponding gene in the evolved strain *S. putrefaciens* G14. Soft-agar assays showed that the spreading phenotype was completely lost in this mutant (Fig. S2). This result indicated that MCP_0387 is directly

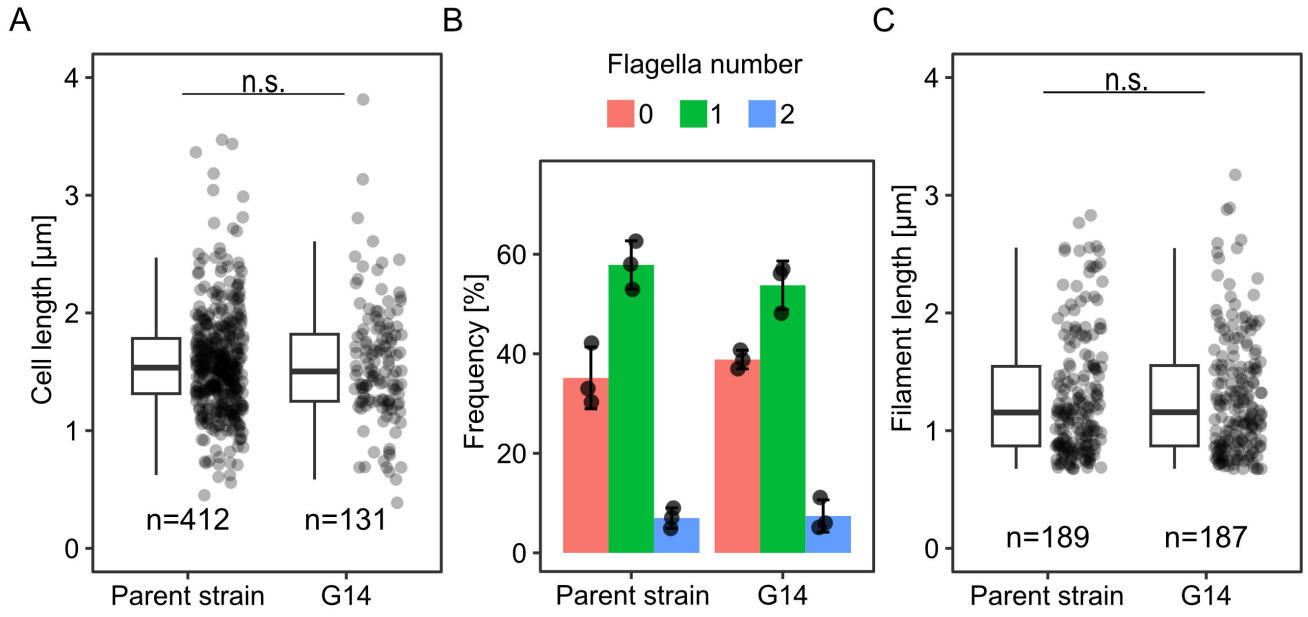

FIG 2 Cell morphology and flagellation of the G14 mutant. Quantification of (A) length of cells, (B) percentage of flagellated cells, and (C) length of filaments, each in liquid media. n.s., not significant according to a pairwise.t.test; the number of cells is indicated by *n*.

involved in the observed spreading phenotype and that the mutation does not abolish the transcription of the MCP_0387-encoding gene.

For further analyses, we introduced a line of mutations into the *S. putrefaciens* wild type to exclude any potential effects of the other mutations we identified through sequencing. First, we constructed a double mutation including the Δ24 deletion mutation along with a deletion of the downstream gene encoding MCP_0387 (Δ24Δ0387). In this strain, Sputcn32_0387 was re-integrated into its native position on the chromosome in *S. putrefaciens* Δ24Δ0387 (*S. putrefaciens* Δ24). Soft-agar spreading assays using the three strains showed that the deletion of the 24 bases upstream of the MCP-encoding gene enhanced the spreading of the mutant cells (Fig. S2). An additional deletion of MCP_0387 abolished the increase in spreading completely, and the strain displayed an even lower spreading than wild-type cells (86.9%). Re-integration of the gene restored the increased spreading phenotype. Based on the results, we proposed that MCP_0387 was mainly responsible for the gain-of-function concerning increased spreading in soft agar.

The identified deletion mutation increases the production of MCP_0387

The 24 bp gene deletion was located upstream of Sputcn32_0387, and deletion of the gene completely abolishes any advantage in spreading and even decreases spreading ability. Therefore, we assumed that, due to the deletion, the transcription activity is affected in a way that leads to a higher abundance of the MCP. To determine the promoter activity, we created a transcriptional fusion to a *lux*-based reporter by placing a *luxCDABE* gene cassette from *Photorhabdus luminescens* into the chromosome directly downstream of Sputcn32_0387. By this, the expression of Sputcn32_0387 could be directly quantified *in vivo* via luminescence emitted by the cells. Compared to the wild-type background, the luminescence of the Δ24 mutant was significantly but only moderately higher (about 116%; Fig. 3B). As the next step, we aimed to enable visualization and quantification of MCP_0387. To this end, we created a Sputcn32_0387-mCherry hybrid gene, which was integrated into the appropriate strains to replace native Sputcn32_0387. This resulted in the production of stable MCP_0387 with a C-terminal

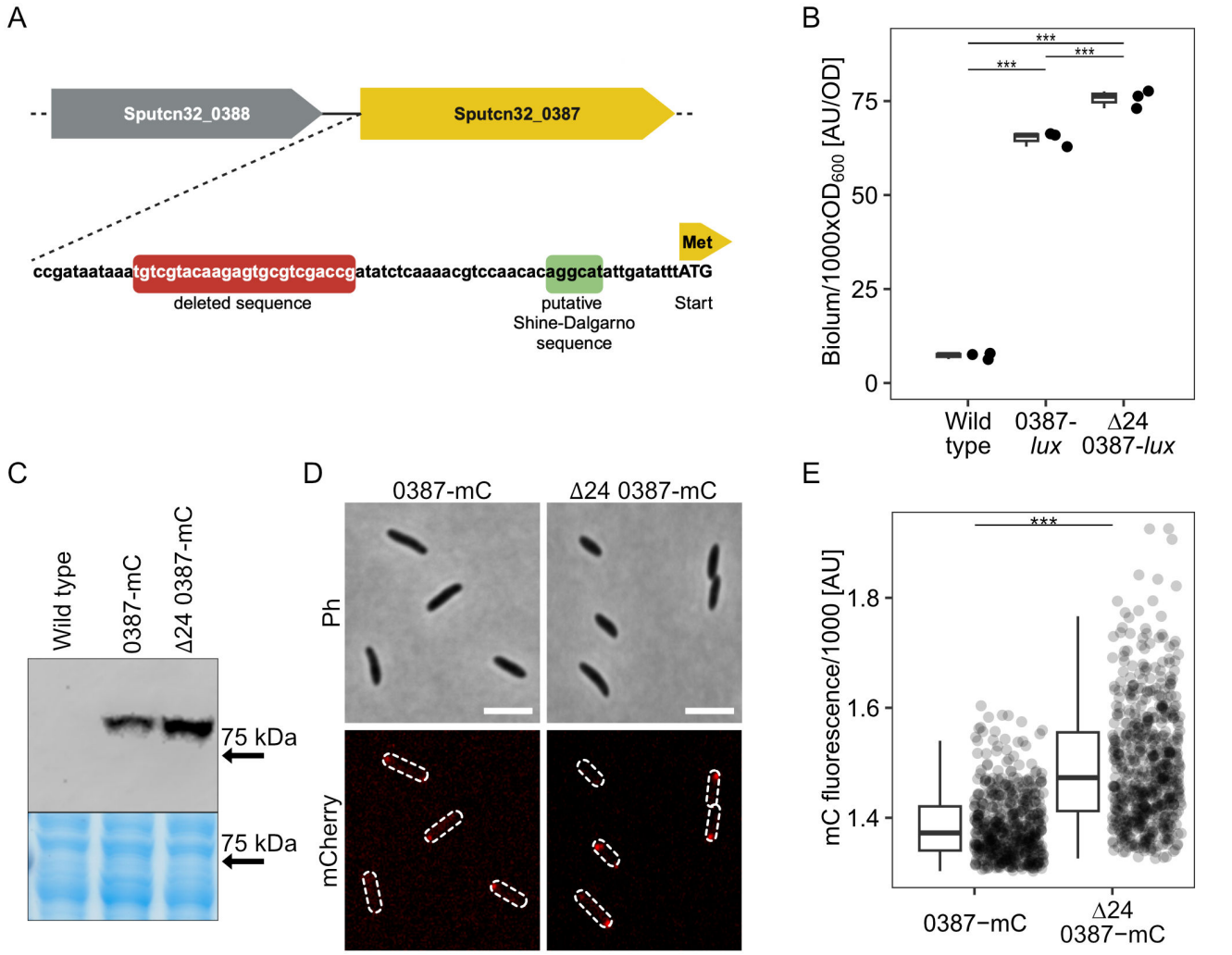

FIG 3 Mapping of the dominant mutation to MCP_0378. (A) Cartoon of gene region. A 24 bp region was found to be deleted upstream of SO_0384, encoding an MCP (MCP_ 384). (B) Quantification of SO_384 expression by integration of *luxCDABE* directly downstream of the structural gene. Light units emitted by the indicated strains were determined in exponentially growing cultures. (C) Comparison of produced MCP_0387-mCherry in the wild type and the Δ24 mutant backgrounds by western blotting. The panel below shows the same region of the Coomassie-stained gel prior to blotting as loading control. For the full uncut gel and western blot, see Fig. S3. (D) Localization of MCP_0387-mCherry by fluorescence microscopy. Shown are micrographs of cells expressing the hybrid fusion gene from the chromosome. The upper two panels show the phase contrast image, and the lower two show the corresponding mCherry fluorescence image, where the position of the cells is outlined. The scale bar equals 5 µm. For an image including the untagged wild type, see Fig. S4. (E) Quantification of the polar mCherry fluorescence intensity. (B and D) The asterisks display the significance using a pairwise.t.test ($P < 0.01$).

fusion to the fluorophore mCherry. Fluorescence microscopy and western blotting showed that MCP_0387-mCherry is produced and polarly localized in all wild-type and Δ24 mutant cells, but the abundance of the MCP is moderately increased in the latter strain by a factor of about 1.5 (Fig. 3C and D; Fig. S3 and S4). We further determined the effect of even higher MCP_0387 levels, and the protein was produced ectopically from a plasmid. We found that, under these conditions, the MCP exerted a negative effect on the spreading ability of the corresponding strain (Fig. S5). From this, we concluded that the deletion leads to only a moderate increase in the production and abundance of the MCP, which in turn enhances spreading in soft agar.

MCP_0387 affects chemotaxis of *S. putrefaciens*

The identification of an MCP as the major contributor to enhanced spreading in soft agar suggested that the observed phenotype is mediated by differences in signal perception during chemotaxis. To first determine if the increased spreading is not due to enhanced swimming speed rather than chemotaxis signaling, we performed three-dimensional (3D) tracking of wild-type, Δ24, and Δ24Δ387 cells under free-swimming conditions. We found that the cells of the three strains displayed similar distributions of instantaneous swimming speeds and that the maximum speed (about 62 μm · s^{-1}) is not different between the strains (Fig. 4A; Fig. S6A shows the distribution of average swimming speeds). The distribution of run durations and tumble frequencies was also highly similar under these conditions (Fig. S6B and C). A previous study focusing on the rheology-dependent swimming of *Vibrio alginolyticus* (36) found that the production of lateral flagella decreased the cells' swimming speeds by around a third. In that study, the cells were grown in viscous media to induce the production of lateral flagella; all of our strains were grown in standard media, with viscosity close to that of water, and we found a modest difference in the average swimming speeds (around 8% between strains) but little difference in the overall distribution of either average or instantaneous speeds. These facts, taken together with the fluorescent labeling experiments showing that the mutant and wild type have similar lateral flagella production, lead us to consider it unlikely that the production of lateral flagella affects the swimming speed here.

Having ruled out swimming speed as the predominant factor for the observed increase in spreading, we reasoned that altering the chemotaxis response by different levels of MCP_387 may be dependent on the environmental nutrient conditions. Therefore, we next determined whether the mutant's phenotype is retained in media other than full-strength LB (Fig. 4B and C). We observed that, in soft-agar spreading assays with decreasing concentrations of LB, the spreading advantage of the mutant was retained at 50% LB. In contrast, the spreading advantage became non-significant in 10% LB, in LM medium (a HEPES-buffered medium containing small amounts of yeast extract and peptone and lactate as main carbon source), or in a buffer with 0.5% casamino acids.

To disentangle the effects of growth, diffusion properties, and chemotaxis, which combine to give rise to a given spreading ability on soft agar, we also probed the drift of the mutants up controlled gradients of the different media, using microfabricated chambers that connect two reservoirs with different concentrations of chemoeffectors via a small rectangular channel (37). For this, we used the Δ24 and the Δ24Δ0387 mutants, between which we expected the largest differences according to the soft-agar spreading assays. The cells start from the low concentration reservoir and drift toward the other reservoir by a combination of diffusive flux and chemotactic bias. The Δ24 and Δ24Δ0387 strains show similar drifts in the absence of initial gradients in LB medium (Fig. 4D), indicating that their diffusion is similar in a liquid medium. In contrast, the Δ24 strain shows a stronger drift in response to a large gradient of LB than the Δ24Δ0387 strain (Fig. 4D). Conversely, both strains have similar drifts in a gradient of casamino acids. Hence, the receptor 0387 is responsible for a specific chemotactic response to LB gradients that contributes to the enhanced spreading of the Δ24 strain on LB soft agar.

MCP_387 levels affect motility in soft agar

To more accurately determine the movement patterns of the MCP_0387 mutant cells as compared to those of wild-type cells, we performed a holographic analysis of motility within the soft-agar matrix. To this end, a soft-agar spreading assay was set up and holographic imaging was performed at the migration front of the spreading halo at a region where the cell density allowed to obtain tracks of single cells. The wild-type parent, the Δ24Δ0387, and the Δ24 were tracked. We observed that, within the soft agar, the cells exhibited periods of frequent directional changes with little overall progress, which were interrupted by longer runs (Fig. 5A). Such a "hop-and-trap" motility has been observed previously for flagellated bacterial cells entrapped in a polysaccharide matrix (38–41). Fig 5 shows stereotypical examples of cell tracks in culture medium (Fig. 5A) and

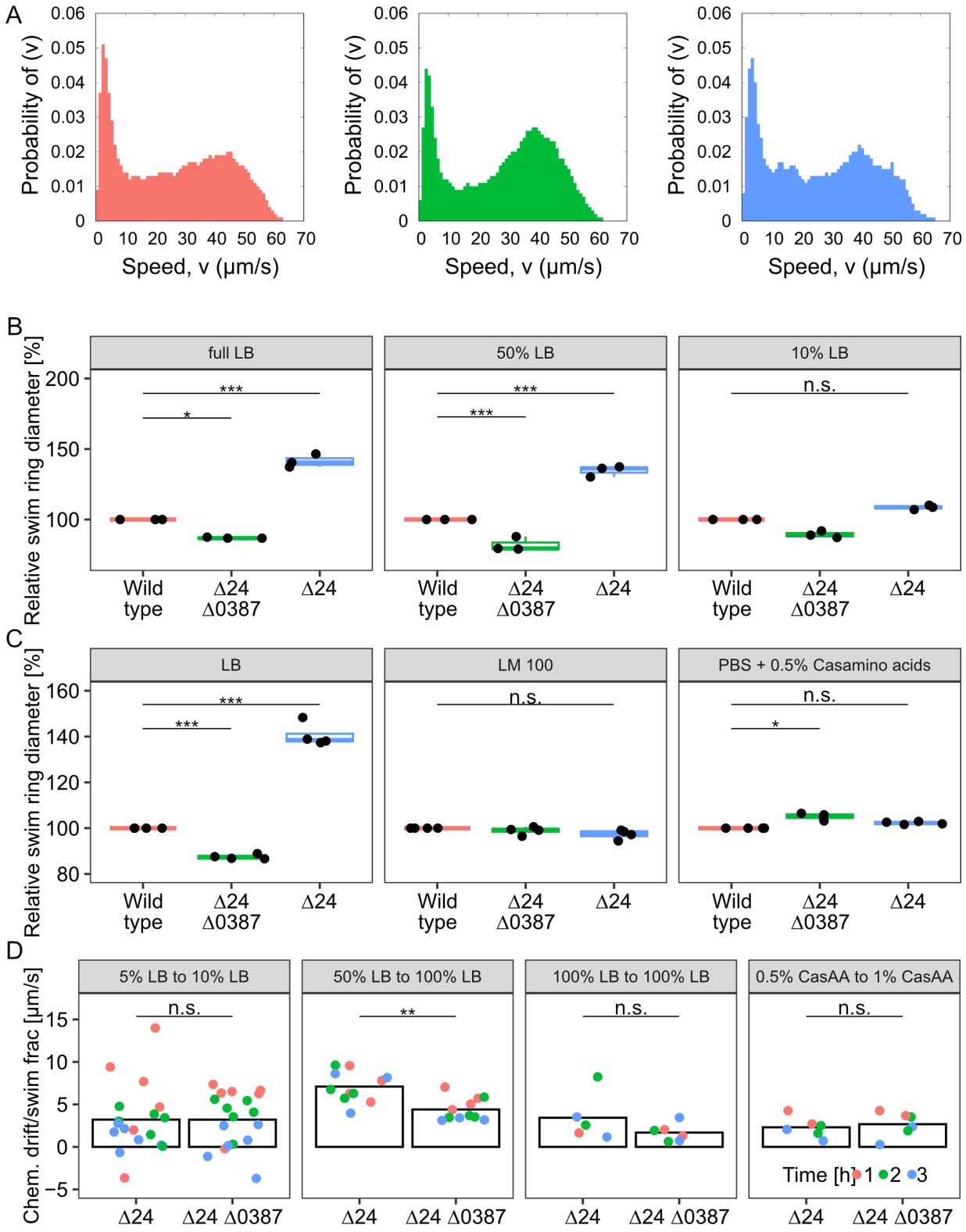

FIG 4 Effects of MCP_0387 levels on chemotaxis. (A) Quantification of the swimming speed during free swimming by 3D tracking. Shown is the speed distribution of the wild type (left panel; red; n = 281), the Δ24Δ0387 mutant (middle panel; green; n = 935), and the Δ24 mutant (right panel; blue; n = 265). (B) Quantification of wild type and mutant spreading at different LB conditions as indicated. Shown are the results from at least three biological replicates.

(Continued on next page)

Fig 4 (Continued)

(C) Quantification of wild type and mutant spreading under different media conditions (LB, LM, and PBS buffer plus casamino acids) as indicated. Shown are the results from at least three biological replicates. (D) Quantification of the chemotactic drift in controlled gradients as indicated. Shown are the results of at least three biological replicates after 1 (red), 2 (green), and 3 (blue) hours of incubation. The asterisks display the significance using a pairwise.t.test (*, $P < 0.05$; ***, $P > 0.01$; n.s., not significant).

in agar (Fig. 5B). We do not find a characteristic length that corresponds to "hops" within the matrix, as might be expected if the surroundings contained structures of a particular size (e.g., the so-called α- and β-relaxation times in colloidal glasses) (42). As a simpler heuristic, we investigated the average and standard deviation of the distance traveled by each cell in 100 ms (i.e., the inverse of the frame rate). The statistics for these "steps" are shown in Fig. 5C and D. The mean and standard deviation in step size are similar between wild type and Δ24Δ0387. In contrast, the Δ24 strain shows longer step sizes and a bias toward larger standard deviation in step size. The mean of the step size shown by

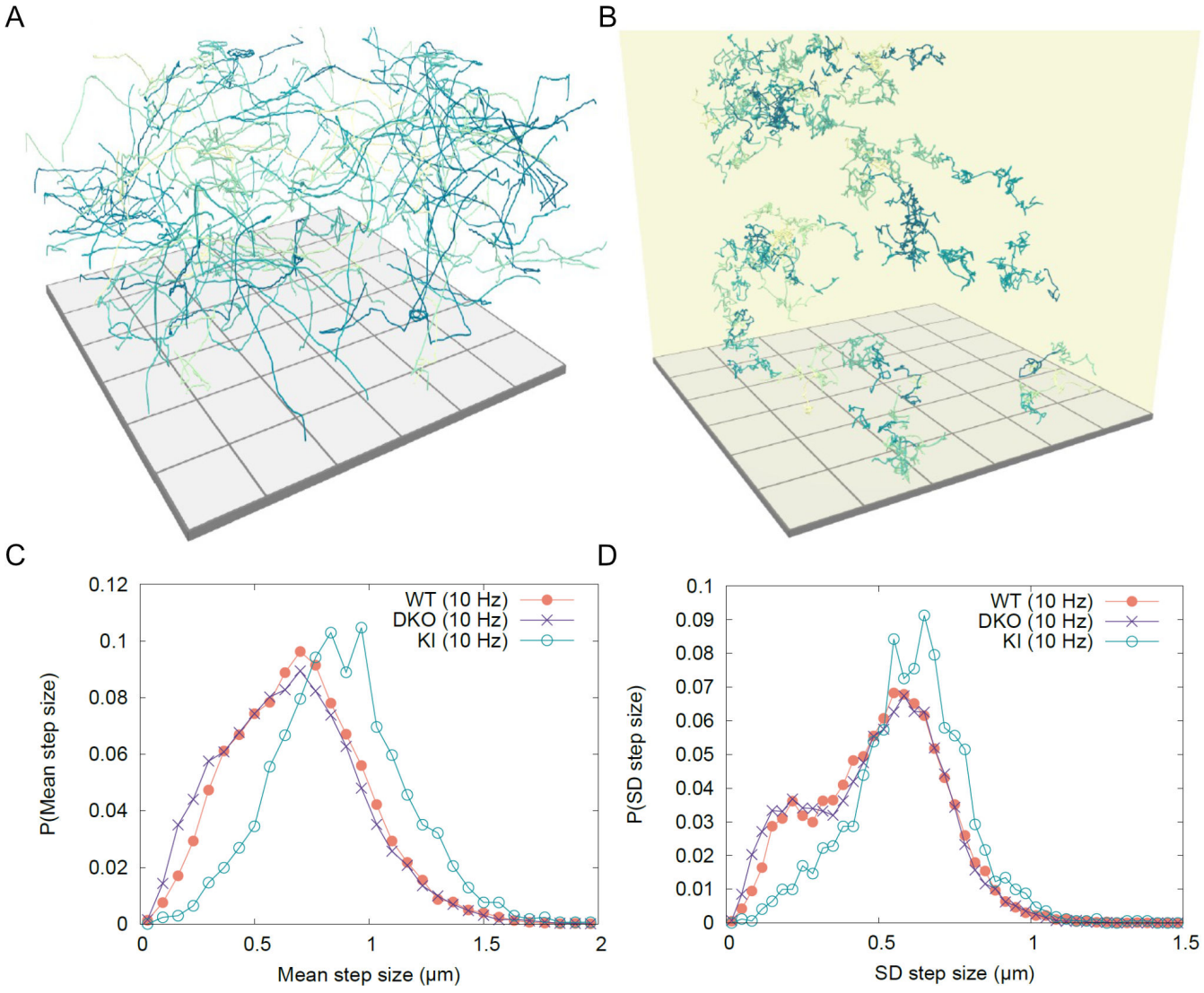

FIG 5 MCP_0387 affects spreading in soft agar. 3D track projection of wild-type cells under planktonic conditions (A) and in soft agar (B). The side of each square at the bottom is 100 µm. (C) The mean distance traveled in 100 ms ("step size") of the indicated cells in soft agar (wild type, red; Δ24Δ0387, green; Δ24, blue). (D) Standard deviation in step size (wild type, red; Δ24Δ0387, green; Δ24, blue). The number of tracks quantified was 9,931 for the wild type, 11,393 for the Δ24Δ0387 mutant, and 1,709 for the Δ24 mutant. Further parameters can be found in Fig. S6 and S7.

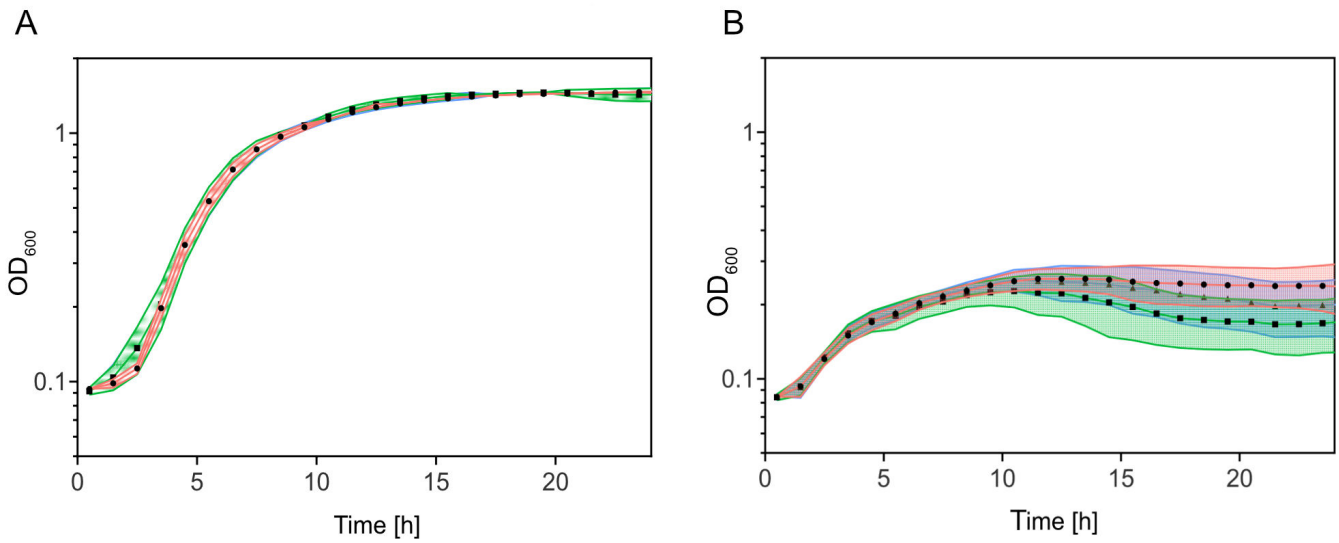

FIG 6 Effect of MCP_0378 levels on growth. Growth of the indicated strains in (A) LB and (B) 4M media. Shown are the results of three biological replicates. The wild type is displayed in red, the Δ24 mutant is in blue, and the Δ24Δ0387 mutant is in green.

Δ24 is around 50% larger than that shown by the wild type, in good agreement with the macroscopic result. Track analyses were also performed to investigate the confinement ratio (net cell displacement divided by track contour length), direction correlation, and directional bias in the cells' movements (Fig. S7), but these show little difference between strains, leaving step size as the dominant contribution to the increase in spreading observed in Δ24.

MCP_387-enhanced spreading does not significantly affect growth

Previous studies showed that experimental evolution of soft-agar spreading or swarming, which was based on increased expression of flagella genes and formation of longer or additional flagella, resulted in a significant decrease in growth under the same conditions. Therefore, we determined whether this would be similarly true for the increased spreading caused by MCP_387. Corresponding growth experiments showed no significant difference between the wild-type and mutant strains in nutrient-rich (LB) medium and in nutrient-limited (4M) medium (Fig. 6).

DISCUSSION

Experimental evolution approaches to bacteria have emerged as a useful tool to study various aspects of adaptation and evolution (43–48). Here, we performed experimental evolution in soft agar using *S. putrefaciens* cells with a dual flagellar system to explore the potential of the underlying regulatory system for mutations beneficial to spreading in complex environments. *S. putrefaciens* shows a complex regulatory interplay between the main polar and secondary lateral flagellar systems under these conditions. However, instead of a general flagellar regulation, a frequently observed evolution path in *E. coli*, we could attribute the better spreading of the enhanced spreading mutant that we obtained to the overproduction of a single chemotaxis sensor protein, MCP_0387. Accordingly, our results demonstrated that the observed phenotype was due to an enhanced chemotactic capability of the mutant strain under appropriate nutrient conditions.

Generally, flagella-mediated motility requires bacteria to balance the fitness trade-off between the benefits of chemotaxis and the costs of allocating cellular resources to motility, and, accordingly, flagella synthesis is subject to intricate regulation at several levels. The trade-off between motility and growth was commonly observed when cells

were experimentally selected for enhanced spreading and chemotaxis (14–16). The mutations causing the up-motile phenotype were usually mapped to factors directly or indirectly involved in flagella regulation. A common mutation that underlies a better-spreading phenotype in *E. coli* strains is the integration of insertion sequence (IS) elements into the regulatory region of the *flhDC* operon, resulting in upregulation of flagella synthesis (49–52). Other studies on the experimental evolution of *E. coli* spreading identified further regulatory key elements, such as the FlgM/FliA checkpoint, that govern flagella formation or length. These mutations affect the swimming speed and, by this, alter the chemotactic drift (16). Similarly, the experimental evolution of a swarmer mutant of monopolarly flagellated *Pseudomonas aeruginosa* identified a mutant in the regulator of the flagellar number, FleN. The isolated FleN mutants form more polar flagella that enable better swarming (i.e., flagella-mediated movement across surfaces) but are negatively affected in growth (53). In our case, the mutation did not occur in a regulatory factor but in the chemotactic sensory system, resulting in a highly environment-dependent upgrade of spreading. Despite its narrow medium specificity, this specialist evolution path does not require the expense of a large protein amount, as would be the case if more or longer flagella were synthesized, which limits the trade-off concerning growth. As we performed the isolation of just one line of mutants, it is not clear if mutation of the chemotaxis system would be the predominant outcome of experimental evolution in *S. putrefaciens* under these conditions. The more complex regulatory network of this species with its two flagellar systems may not as readily evolve as that of *E. coli*. Alternatively, a fine-tuning of environment perception via receptor level changes might be easier for a species that has many more receptors than *E. coli*. More parallel lines of evolved *S. putrefaciens* strains under different environmental conditions are required to address this question in future experiments.

MCP_0387 is only one out of 36 potential MCPs, which indicates a large chemotactic sensory repertoire of *S. putrefaciens*. The level of its overproduction in the spontaneous mutant is rather small (a factor of 1.2–1.5), while ectopic production at higher levels rather negatively affects spreading. So how can such a small increase in MCP abundance have such a pronounced consequence? Previous studies showed that MCPs form trimers of dimers, which assemble into large well-structured arrays harboring the different MCPs (54). The composition of the chemotaxis cluster is usually heterogeneous, as the abundance of different MCPs in the arrays can be vastly different. In *E. coli*, the number of Tsr and Tar receptors exceeds that of the Trg and Tap receptors by a factor of 10 (55–57). Also in *Bacillus subtilis* and *Sinorhizobium meliloti,* the stoichiometry of the different MCPs is highly different (58, 59). The tight and organized clustering enables and facilitates cooperativity and signal processing so that diverse signals can be processed and enhanced (60–64). It has been demonstrated previously that shifting the balance of MCP abundance, e.g., by overproduction, alters the chemotactic sensitivity toward the corresponding signal (65–68). Notably, the effect appears to be smaller for MCPs that are already present at high abundance (69). Accordingly, it has been shown for diverse species that the MCP abundance can be adjusted to the environmental conditions (70, 71) and by the presence of the corresponding chemoeffector (72–76). It remains to be shown if this is also the case for MCP_0387. A recent study on *E. coli* migration through soft agar demonstrated that cells isolated from the migration front tend to possess higher levels of the MCP Tsr, but only when the corresponding ligand serine was present (77). In contrast to the case described here for *S. putrefaciens* MCP_0387, the elevated Tsr levels occurred as the result of general heterogeneity in Tsr production in an *E. coli* population. Due to their ability to better chase the self-created traveling serine concentration gradient, these cells are then moving toward the front of the spreading zone (77, 78). It is conceivable that such heterogeneity in MCP levels similarly occurs in *S. putrefaciens*, albeit with 36 instead of just five MCPs, and that, by permanently increasing average levels, the mutation enriches the population in cells with higher expression of MCP_0387 that may play a similar pioneering role very efficiently in our conditions. However, a too high production of MCP_0387 may interfere with efficient

signal transduction in complex environments, resulting in the observed decrease in spreading upon MCP overproduction. It is not yet clear how the deletion within the gene region upstream of Sputcn32_0387 affects the transcription activity of the gene, as promoter regions in *Shewanella* sp. are poorly conserved and therefore hard to predict (32, 79). Whether the deletion improves sigma-factor recognition or alters regulator binding or structures in the non-translated region requires further studies.

Generally, the chemotactic potential of *Shewanella* sp. has only started to be explored, and so far, the signal the MCP responds to remains unknown. Notably, close homologs to MCP_0387 are widespread among *Shewanella* species, suggesting that the signal can be sensed and responded to by a number of these ubiquitously occurring bacteria. A potential orthologue of MCP_0387 in *S. oneidensis* MR-1, SO_4454 (92% identity/95% positives), had been implicated as a potential candidate for energy taxis in this species; however, the effect was minor (80). The periplasmic domain of MCP_0387 harbors a Cache domain, which comprises the largest superfamily of extracellular sensors. The domain present in MCP_0387 is predicted to belong to the less abundant Cache_3-Cache_2 subfamily (81). Cache domains have been implicated in binding a large range of potential ligands that may occur in the complex media containing tryptone and yeast extract, where the up-motile phenotype was visible. An analysis of the sensing MCP's sensor domain did not give any direct hints with respect to potential ligands, and so far, none of the potential ligands we tested (e.g., amino acids, small peptides) have given any clue (unpublished observations). The nature of the signal that *S. putrefaciens* and likely other *Shewanella* species respond to via MCP_0387 and the corresponding potential orthologues is the subject of current studies.

The chemotactic swimming pattern of bacteria at the single-cell level has mainly been studied in detail during free swimming in planktonic environments. However, the movement pattern of single cells in structured environments differs substantially from that of their free-swimming counterparts (38, 82–85). Under free-swimming conditions, the movement phases ("runs") are interrupted by short reorientation events. In contrast, when moving through soft agar, cells tend to be stalled for longer periods of time between runs. It is assumed that the cells are trapped in a pore within the polysaccharide matrix and require some reorientation events until an opening within the pore allows another run (38–41). The 3D tracking in this study showed that *S. putrefaciens* cells perform a similar "hopping and trapping" movement (39) in soft agar (see Fig. 5B). We found that the *S. putrefaciens* up-motile mutants are biased toward longer runs, as would be expected for an enhanced chemotaxis response. In addition, the mutant cells tend to spend a shorter time in the trapped mode. For *E. coli*, the likelihood of leaving the trap is thought to depend on the successful reorientation of the cell, the "tumble," which is affected by the geometry of the pore (39). In contrast, *S. putrefaciens* and other polarly flagellated species navigate by a run-reverse-flick pattern, and flagellar wrapping and lateral flagella activity may assist in leaving the trap (8, 27, 31, 33). In addition, diffusion and, therefore, local nutrient concentrations may be different under these conditions. Further studies are required to determine flagellar behavior and identify the exact mechanism underlying the shorter periods of the *S. putrefaciens* MCP_0387 mutant in the trapped state in soft agar.

MATERIALS AND METHODS

Growth conditions and media

E. coli and *S. putrefaciens* CN-32 strains used in this study are listed in Table S1. Unless specified otherwise, cells were cultured in LB medium at 30°C (*S. putrefaciens*) and 37°C (*E. coli*). Kanamycin and 2,6-diaminoheptanedioic acid were used as selection markers at final concentrations of 50 mg mL^{-1} and 300 µM, respectively.

Growth experiments of *S. putrefaciens* strains were carried out in 1 mL LB or 4M (86) medium at 30°C in a 24-well microtiter plate using a BioTek Epoch 2 Microplate

Spectrophotometer (Agilent). Each experiment was carried out in at least three biological replicates with four technical replicates each.

Strain constructions

All *S. putrefaciens* modifications were constructed as outlined previously (26). In brief, double homologous recombination was applied using 500 bp flanking regions upstream and downstream of the target region to generate open reading frame deletions or integrate open reading frames with point mutations or genetic markers. Recombination was achieved using the suicide plasmid pNPTS-R6K (87) after conjugation from *E. coli* WM3064 as listed in Table S2. Vectors were constructed using standard Gibson assembly protocols (88) using primers listed in Table S3.

Soft-agar spreading assays

Soft agar was prepared using 0.25% (wt/vol) select agar (Invitrogen) in LB medium, lactate medium (LM100) (89), or PBS supplemented with 0.5% (wt/vol) casamino acids (Carl Roth). The soft-agar plates were inoculated with strains pre-grown to exponential growth phase and incubated at 30°C overnight. Strains to be directly compared were always inoculated on the same plate.

Time-lapse experiments of soft-agar spreading assays were performed using Epson Perfection V39 scanners. Image series were recorded using the scanlag software (90). Each petri dish was inoculated with a single colony and incubated at 30°C for 18 hours while all assays were scanned in 15 minutes time intervals. Each image series was analyzed using Fiji ImageJ (version 1.54i). To this end, the image series was converted to an image stack where the 0 minute image was used for background subtraction. Images were converted to 8-bit, and a median filter (5 pixels) was applied. Colony outlines were segmented by applying the "threshold triangle" method and quantified by the "analyze particle" functions.

Spreading evolution assay

For spreading evolution experiments, strain S8493 was used to perform repeated soft-agar spreading assays in 0.25% select agar in LB medium under standard conditions. Cells were harvested from the motility front by careful pipetting and were used to re-inoculate the consecutive spreading assay. After 14 cycles, cells harvested from the motility front were used to inoculate fresh LB medium to prepare cryo stocks in 10% DMSO to be stored at −80°C.

Flagellar filament labeling and microscopy

In order to visualize flagellar filaments, surface-exposed threonine residues of the flagellin monomers were exchanged to cysteine as outlined previously (27, 31). For microscopy, cells were harvested from soft-agar spreading assays by excising the agar fragment bearing the motility front and incubating it in PBS for 5 min. The cell suspension was separated from agar fragments, centrifuged (1,200 × *g*, 5 min, room temperature), and resuspended in 50 µL PBS. Filament staining was performed by applying 2 µL Alexa Fluor 488 C5 maleimide (Thermo Fisher Scientific) for 18 min in the dark. Cells were washed with 1 mL PBS and sedimented by centrifugation three times. Stained cells were applied to agarose patches (1% [vol/vol] select agar in PBS) for microscopy using a custom microscope setup (Visitron Systems) based on a Leica DMI 6000 B inverse microscope (Leica) equipped with a pco.edge sCMOS camera (PCO), a SPECTRA light engine (lumencor), and an HCPL APO ×63/1.4–0.6 objective (Leica) using a custom filter set (T495lpxr, ET525/50m; Chroma Technology). For phase contrast and fluorescence microscopy, 50 ms exposure times were used.

Cell body measurements were performed based on phase contrast images using the BacStalk software (version 1.8) (91). Filament measurements were performed using fluorescent microscopy images using Fiji ImageJ (version 1.54i). Filaments were

segmented on images using the gray value 2,000 as the threshold for background subtraction and the "convert to mask" functions. Object lengths were measured using the "skeletonize (2D/3D)" and "analyze skeleton (2D/3D)" functions.

Strain sequencing

Chromosomal DNA was extracted using the E.Z.N.A. Bacterial DNA kit (Omega BIO-TEK) according to the manual instructions appropriate for Gram-negative bacteria. From extracted genomic DNA, TruSeq PCR-free sequencing libraries (Illumina, San Diego, USA) were generated according to the manufacturers' instructions and sequenced on an Illumina MiSeq machine (2 × 300 bp) with V3 chemistry. Separate libraries were generated for the parental strain as well as two descending strains after 14 generations of selection. Reads were imported into Geneious Prime 2022.0.1 (https://www.geneious.com) and analyzed using the pre-defined "Map reads then find variations/SNPs" workflow. Detected variants against the *S. putrefaciens* CN-32 reference (GenBank: CP000681.1) were then exported for further filtering and analysis.

Chemotaxis experiments in liquid medium

Chemotactic drift measurements were performed similarly to previous works with *E. coli* (92) and *V. cholerae* (93). In short, PDMS microchambers were constructed by molding Sylgard 184 (Dow Corning) mixed in a 10:1 base-to-crosslinker ratio on a SU8-based Silicon wafer template, curing overnight at 65°C, peeling off and cutting the hardened PDMS to shape, and binding it to a glass slide via oxygen plasma treatment. The chambers were filled with DI sterile water 20 minutes after production to preserve the hydrophilicity of their surfaces until same-day use. The microchamber consists of two large reservoirs connected by a small channel (L × W × H = 2 mm × 1 mm × 70 µm). The first reservoir receives a first solution of the indicated composition, which contains bacteria at 10^8–10^9 cells/mL concentration, while the second reservoir is filled with a second solution, which is initially cell free. After filling the device and sealing it, a gradient of concentrations forms in the channel, which reaches a steady-state profile in 1 h in the absence of consumption. We measure the drift of the cells in this gradient 1, 2, and 3 h after sealing in the middle of the channel at mid-height under a phase contrast microscope (Nikon *Ti*) with a ×10 (NA 0.3) objective and a CMOS camera (Mikrotron Eosens CXP, 1 px = 1.4 µm) that records a movie at 200 frames/s for 100 s.

The movie is analyzed using dynamic differential microscopy (DDM) (94) to measure swimming speed v_0 and fraction of swimming cells φ and using phase differential microscopy (ϕDM) (37) to measure population-averaged drift v_d as described previously. The algorithms are implemented as publicly available ImageJ Plugins (92). In DDM, the differential intermediate scattering function is computed from the spatial Fourier components of the images. It is then fitted with a model that accounts for a mixed population of diffusing non-motile cells and motile cells, which are modeled as 3D swimmers with swimming speed taken from a Schultz distribution (94). The average swimming speed v_0 and the fraction of swimmers φ are then determined as the average value of the fitted parameter on the range of wave numbers where the fit converges (typically, q = [0.5, 2.0] px^{-1}). In ϕDM, the mean drift R(t) of the population of cells is extracted from the shift in the phase of the Fourier components as described previously (37). A linear fit of the drift over the whole movie yields the population-averaged drift velocity v_d. Since the drift of non-swimmers is negligible, the (chemotactic) drift of the motile cells is estimated as $v_{ch} = v_d/\varphi$.

Holographic microscopy data acquisition

Digital holographic microscopy was configured as described previously (33, 95, 96). In brief, a single-mode optical fiber was held in the condenser mount of an inverted microscope, and the light directed down onto the sample stage. Samples were imaged using a ×20 magnification objective lens and a Mikrotron MC-1362 camera, resulting in a

final magnification of 0.70 µm per pixel. Videos were acquired at a resolution of 1,024 × 1,024 pixels and frame rates of 10 Hz or 20 Hz for cells embedded in agar and 100 Hz for the planktonic analysis.

Planktonic samples

Tracking experiments in liquid medium were performed with cells during the exponential growth phase diluted to an optical density of 0.1 at 600 nm with fresh LB medium. The samples were contained in chambers constructed from glass slides and UV-curing glue to provide a volume measuring approximately 5 × 20 × 0.3 mm^3. Samples were loaded by capillary action from one end and sealed with petroleum jelly to prevent evaporation. Three movies were acquired from each strain. The movies were detrended by subtracting a fitted fourth order polynomial function to the intensity series of each pixel; this removes static background artifacts, as well as any slow drifts in the sample, but maintains the images of the motile cells. Each frame of these detrended movies yielded a three-dimensional reconstruction of the optical field within the sample. The field was reconstructed using Rayleigh-Sommerfeld back-propagation (97), creating stacks of numerically reconstructed images from each raw data frame. The optical field in the sample was reconstructed in around 100 axial planes uniformly separated by 3 µm throughout the sample volume, and image stacks were segmented based on axial intensity gradients (98, 99). Each video frame was processed independently to allow parallelization, with coordinates in subsequent frames linked together across time to make cell tracks. Motile and non-motile cells were distinguished using their mean-squared displacements (MSDs). Objects were identified as non-motile and discarded if their average MSD per unit time or if average squared displacement at one second was too low. Tracks were regularized using piecewise cubic splines to obtain better estimates of instantaneous swimming speed. Cell reorientations ("tumbles") were identified as peaks in angular velocity, and the time between consecutive reorientation events was taken to be the duration of one run. Tracks must contain at least two reorientation events to contribute to the run duration statistics.

Agar samples

For 3D holography tracking experiments of cells in agar, all strains were cultured under standard conditions as outlined for soft-agar plates. The samples were imaged on an inverted microscope in the same manner as the planktonic ones, with the plate lid removed while the video sequences were obtained. Detrending of the video sequences to remove background artifacts was performed as in the planktonic case. The optical field was reconstructed using 250 axial slices of 3 µm, giving a total sample volume of 720 × 720 × 750 $µm^3$ within the agar, but the post-processing was otherwise the same as in the planktonic case.

The tracks within the agar matrix were quantified by measuring their step size (distance traveled in 100 ms), "confinement ratio" (derived from the similar metric used in the TrackMate ImageJ plugin [100], direction correlation, and the anisotropy in motility). The step size was chosen as the distance traveled between frames when imaging at 10 Hz. The confinement ratio of a track is defined as its contour length divided by its end-to-end distance. The direction correlation is defined as $\langle \mathbf{T}(t+\tau) \cdot \mathbf{T}(t) \rangle$, where $\mathbf{T}(t)$ is the unit tangent vector to the trajectory at time t, and $\mathbf{T}(t+\tau)$ is the tangent vector after subsequent delay time τ. The angle brackets indicate an average over initial times, t. The anisotropy in motility was assessed by examining the end-to-end vector (net displacement) for each track and binning these vectors into 10 azimuthal directions, as shown in Fig. S7. The distance of each marker from the origin denotes the probability of finding a net displacement in each direction.

Statistical analysis

Statistical tests were performed using the pairwise.t.test function of R statistical language (version 4.2.2). For calculations, two-sided, non-pooled standard deviations, unpaired were set as parameters. *P* value adjustments were calculated according to the Benjamini-Hochberg correction method.

ACKNOWLEDGMENTS

This work was supported by a grant from the Deutsche Forschungsgemeinschaft DFG (TH831/8-1) to K.M.T. R.C. acknowledges support from DFG grant CO1813/2-1.

AUTHOR AFFILIATIONS

[1]Institut für Mikrobiologie und Molekularbiologie, Justus-Liebig-Universität Gießen, Gießen, Germany
[2]Department of Physics, University of York, York, United Kingdom
[3]Max Planck Institute for Terrestrial Microbiology, and Center for Synthetic Microbiology (SYNMIKRO), Marburg, Germany
[4]Center for Biotechnology, Bielefeld University, Bielefeld, Germany

AUTHOR ORCIDs

Jörn Kalinowski http://orcid.org/0000-0002-9052-1998
Kai M. Thormann http://orcid.org/0000-0001-7292-4884

FUNDING

Funder	Grant(s)	Author(s)
Deutsche Forschungsgemeinschaft	TH831/8-1	Kai M. Thormann
Deutsche Forschungsgemeinschaft	CO1813/2-1	Rémy Colin

AUTHOR CONTRIBUTIONS

Daniel B. Edelmann, Conceptualization, Data curation, Investigation, Methodology, Validation, Visualization, Writing – original draft, Writing – review and editing | Anna M. Jakob, Investigation, Methodology | Laurence G. Wilson, Conceptualization, Data curation, Formal analysis, Investigation, Methodology, Visualization, Writing – original draft, Writing – review and editing | Rémy Colin, Conceptualization, Formal analysis, Funding acquisition, Investigation, Supervision, Validation, Writing – original draft, Writing – review and editing | David Brandt, Data curation, Formal analysis, Investigation, Methodology, Writing – original draft, Writing – review and editing | Frederik Eck, Investigation, Methodology, Writing – original draft, Writing – review and editing | Jörn Kalinowski, Investigation, Methodology | Kai M. Thormann, Conceptualization, Funding acquisition, Investigation, Methodology, Project administration, Supervision, Writing – original draft, Writing – review and editing

ADDITIONAL FILES

The following material is available online.

Supplemental Material

File S1 (AEM00229-25-s0001.xlsx). Table containing the mutations identified by strain sequencing.
Supplemental material (AEM00229-25-s0002.pdf). Tables S1 to S3 and Figures S1 to S7.
Movie S1 (AEM00229-25-s0003.mp4). Time-lapse scanning recording of soft-agar spreading assays using the indicated strains.

REFERENCES

1. Berg HC, Anderson RA. 1973. Bacteria swim by rotating their flagellar filaments. Nature 245:380–382. https://doi.org/10.1038/245380a0
2. Kearns DB. 2010. A field guide to bacterial swarming motility. Nat Rev Microbiol 8:634–644. https://doi.org/10.1038/nrmicro2405
3. Wadhwa N, Berg HC. 2022. Bacterial motility: machinery and mechanisms. Nat Rev Microbiol 20:161–173. https://doi.org/10.1038/s41579-021-00626-4
4. Matilla MA, Gavira JA, Krell T. 2023. Accessing nutrients as the primary benefit arising from chemotaxis. Curr Opin Microbiol 75:102358. https://doi.org/10.1016/j.mib.2023.102358
5. Sourjik V, Wingreen NS. 2012. Responding to chemical gradients: bacterial chemotaxis. Curr Opin Cell Biol 24:262–268. https://doi.org/10.1016/j.ceb.2011.11.008
6. Bi S, Sourjik V. 2018. Stimulus sensing and signal processing in bacterial chemotaxis. Curr Opin Microbiol 45:22–29. https://doi.org/10.1016/j.mib.2018.02.002
7. Grognot M, Taute KM. 2021. More than propellers: how flagella shape bacterial motility behaviors. Curr Opin Microbiol 61:73–81. https://doi.org/10.1016/j.mib.2021.02.005
8. Thormann KM, Beta C, Kühn MJ. 2022. Wrapped up: the motility of polarly flagellated bacteria. Annu Rev Microbiol 76:349–367. https://doi.org/10.1146/annurev-micro-041122-101032
9. Berg HC. 2003. The rotary motor of bacterial flagella. Annu Rev Biochem 72:19–54. https://doi.org/10.1146/annurev.biochem.72.121801.161737
10. Martínez-García E, Nikel PI, Chavarría M, de Lorenzo V. 2014. The metabolic cost of flagellar motion in *Pseudomonas putida* KT2440. Environ Microbiol 16:291–303. https://doi.org/10.1111/1462-2920.12309
11. Ziegler M, Takors R. 2020. Reduced and minimal cell factories in bioprocesses: towards a streamlined chassis, p 1–44. In Lara AR, Gosset G (ed), Minimal cells: design, construction, biotechnological applications. Springer International Publishing, Cham.
12. Schavemaker PE, Lynch M. 2022. Flagellar energy costs across the tree of life. Elife 11:e77266. https://doi.org/10.7554/eLife.77266
13. Taylor JR, Stocker R. 2012. Trade-offs of chemotactic foraging in turbulent water. Science 338:675–679. https://doi.org/10.1126/science.1219417
14. Yi X, Dean AM. 2016. Phenotypic plasticity as an adaptation to a functional trade-off. Elife 5:e19307. https://doi.org/10.7554/eLife.19307
15. Fraebel DT, Mickalide H, Schnitkey D, Merritt J, Kuhlman TE, Kuehn S. 2017. Environment determines evolutionary trajectory in a constrained phenotypic space. Elife 6:e24669. https://doi.org/10.7554/eLife.24669
16. Ni B, Ghosh B, Paldy FS, Colin R, Heimerl T, Sourjik V. 2017. Evolutionary remodeling of bacterial motility checkpoint control. Cell Rep 18:866–877. https://doi.org/10.1016/j.celrep.2016.12.088
17. Ni B, Colin R, Link H, Endres RG, Sourjik V. 2020. Growth-rate dependent resource investment in bacterial motile behavior quantitatively follows potential benefit of chemotaxis. Proc Natl Acad Sci USA 117:595–601. https://doi.org/10.1073/pnas.1910849117
18. Colin R, Ni B, Laganenka L, Sourjik V. 2021. Multiple functions of flagellar motility and chemotaxis in bacterial physiology. FEMS Microbiol Rev 45:fuab038. https://doi.org/10.1093/femsre/fuab038
19. Amsler CD, Cho M, Matsumura P. 1993. Multiple factors underlying the maximum motility of *Escherichia coli* as cultures enter post-exponential growth. J Bacteriol 175:6238–6244. https://doi.org/10.1128/jb.175.19.6238-6244.1993
20. Chevance FFV, Hughes KT. 2008. Coordinating assembly of a bacterial macromolecular machine. Nat Rev Microbiol 6:455–465. https://doi.org/10.1038/nrmicro1887
21. Guttenplan SB, Shaw S, Kearns DB. 2013. The cell biology of peritrichous flagella in *Bacillus subtilis*. Mol Microbiol 87:211–229. https://doi.org/10.1111/mmi.12103
22. Prüß BM. 2017. Involvement of two-component signaling on bacterial motility and biofilm development. J Bacteriol 199:e00259-17. https://doi.org/10.1128/JB.00259-17
23. Adler J, Templeton B. 1967. The effect of environmental conditions on the motility of *Escherichia coli*. J Gen Microbiol 46:175–184. https://doi.org/10.1099/00221287-46-2-175
24. You C, Okano H, Hui S, Zhang Z, Kim M, Gunderson CW, Wang Y-P, Lenz P, Yan D, Hwa T. 2013. Coordination of bacterial proteome with metabolism by cyclic AMP signalling. Nature 500:301–306. https://doi.org/10.1038/nature12446
25. Hui S, Silverman JM, Chen SS, Erickson DW, Basan M, Wang J, Hwa T, Williamson JR. 2015. Quantitative proteomic analysis reveals a simple strategy of global resource allocation in bacteria. Mol Syst Biol 11:784. https://doi.org/10.15252/msb.20145697
26. Bubendorfer S, Held S, Windel N, Paulick A, Klingl A, Thormann KM. 2012. Specificity of motor components in the dual flagellar system of *Shewanella putrefaciens* CN-32. Mol Microbiol 83:335–350. https://doi.org/10.1111/j.1365-2958.2011.07934.x
27. Kühn MJ, Schmidt FK, Eckhardt B, Thormann KM. 2017. Bacteria exploit a polymorphic instability of the flagellar filament to escape from traps. Proc Natl Acad Sci USA 114:6340–6345. https://doi.org/10.1073/pnas.1701644114
28. Rossmann F, Brenzinger S, Knauer C, Dörrich AK, Bubendorfer S, Ruppert U, Bange G, Thormann KM. 2015. The role of FlhF and HubP as polar landmark proteins in *Shewanella putrefaciens* CN-32. Mol Microbiol 98:727–742. https://doi.org/10.1111/mmi.13152
29. Kojima M, Kubo R, Yakushi T, Homma M, Kawagishi I. 2007. The bidirectional polar and unidirectional lateral flagellar motors of *Vibrio alginolyticus* are controlled by a single CheY species. Mol Microbiol 64:57–67. https://doi.org/10.1111/j.1365-2958.2007.05623.x
30. Bubendorfer S, Koltai M, Rossmann F, Sourjik V, Thormann KM. 2014. Secondary bacterial flagellar system improves bacterial spreading by increasing the directional persistence of swimming. Proc Natl Acad Sci USA 111:11485–11490. https://doi.org/10.1073/pnas.1405820111
31. Kühn MJ, Edelmann DB, Thormann KM. 2022. Polar flagellar wrapping and lateral flagella jointly contribute to *Shewanella putrefaciens* environmental spreading. Environ Microbiol 24:5911–5923. https://doi.org/10.1111/1462-2920.16107
32. Schwan M, Khaledi A, Willger S, Papenfort K, Glatter T, Häußler S, Thormann KM. 2022. FlrA-independent production of flagellar proteins is required for proper flagellation in *Shewanella putrefaciens*. Mol Microbiol 118:670–682. https://doi.org/10.1111/mmi.14993
33. Kühn MJ, Schmidt FK, Farthing NE, Rossmann FM, Helm B, Wilson LG, Eckhardt B, Thormann KM. 2018. Spatial arrangement of several flagellins within bacterial flagella improves motility in different environments. Nat Commun 9:5369. https://doi.org/10.1038/s41467-018-07802-w
34. Pecina A, Schwan M, Blagotinsek V, Rick T, Klüber P, Leonhard T, Bange G, Thormann KM. 2021. The stand-alone PilZ-domain protein MotL specifically regulates the activity of the secondary lateral flagellar system in *Shewanella putrefaciens*. Front Microbiol 12:668892. https://doi.org/10.3389/fmicb.2021.668892
35. Rick T, Kreiling V, Höing A, Fiedler S, Glatter T, Steinchen W, Hochberg G, Bähre H, Seifert R, Bange G, Knauer SK, Graumann PL, Thormann KM. 2022. GGDEF domain as spatial on-switch for a phosphodiesterase by interaction with landmark protein HubP. NPJ Biofilms Microbiomes 8:35. https://doi.org/10.1038/s41522-022-00297-w
36. Atsumi T, Maekawa Y, Yamada T, Kawagishi I, Imae Y, Homma M. 1996. Effect of viscosity on swimming by the lateral and polar flagella of *Vibrio alginolyticus*. J Bacteriol 178:5024–5026. https://doi.org/10.1128/jb.178.16.5024-5026.1996
37. Colin R, Zhang R, Wilson LG. 2014. Fast, high-throughput measurement of collective behaviour in a bacterial population. J R Soc Interface 11:20140486. https://doi.org/10.1098/rsif.2014.0486
38. Wolfe AJ, Berg HC. 1989. Migration of bacteria in semisolid agar. Proc Natl Acad Sci USA 86:6973–6977. https://doi.org/10.1073/pnas.86.18.6973
39. Bhattacharjee T, Datta SS. 2019. Bacterial hopping and trapping in porous media. Nat Commun 10:2075. https://doi.org/10.1038/s41467-019-10115-1
40. Bhattacharjee T, Datta SS. 2019. Confinement and activity regulate bacterial motion in porous media. Soft Matter 15:9920–9930. https://doi.org/10.1039/C9SM01735F
41. Grognot M, Nam JW, Elson LE, Taute KM. 2023. Physiological adaptation in flagellar architecture improves *Vibrio alginolyticus* chemotaxis in complex environments. Proc Natl Acad Sci USA 120:e2301873120. https://doi.org/10.1073/pnas.2301873120
42. Weeks ER, Crocker JC, Levitt AC, Schofield A, Weitz DA. 2000. Three-dimensional direct imaging of structural relaxation near the colloidal

glass transition. Science 287:627–631. https://doi.org/10.1126/science.287.5453.627
43. Fry JD. 2003. Detecting ecological trade-offs using selection experiments. Ecology 84:1672–1678. https://doi.org/10.1890/0012-9658(2003)084[1672:DETUSE]2.0.CO;2
44. Perfeito L, Fernandes L, Mota C, Gordo I. 2007. Adaptive mutations in bacteria: high rate and small effects. Science 317:813–815. https://doi.org/10.1126/science.1142284
45. Kawecki TJ, Lenski RE, Ebert D, Hollis B, Olivieri I, Whitlock MC. 2012. Experimental evolution. Trends Ecol Evol 27:547–560. https://doi.org/10.1016/j.tree.2012.06.001
46. Taute KM, Gude S, Nghe P, Tans SJ. 2014. Evolutionary constraints in variable environments, from proteins to networks. Trends Genet 30:192–198. https://doi.org/10.1016/j.tig.2014.04.003
47. Ferenci T. 2016. Trade-off mechanisms shaping the diversity of bacteria. Trends Microbiol 24:209–223. https://doi.org/10.1016/j.tim.2015.11.009
48. McDonald MJ. 2019. Microbial experimental evolution - a proving ground for evolutionary theory and a tool for discovery. EMBO Rep 20:e46992. https://doi.org/10.15252/embr.201846992
49. Barker CS, Prüss BM, Matsumura P. 2004. Increased motility of *Escherichia coli* by insertion sequence element integration into the regulatory region of the *flhD* operon. J Bacteriol 186:7529–7537. https://doi.org/10.1128/JB.186.22.7529-7537.2004
50. Wang X, Wood TK. 2011. IS5 inserts upstream of the master motility operon flhDC in a quasi-Lamarckian way. ISME J 5:1517–1525. https://doi.org/10.1038/ismej.2011.27
51. Lee C, Park C. 2013. Mutations upregulating the flhDC operon of *Escherichia coli* K-12. J Microbiol 51:140–144. https://doi.org/10.1007/s12275-013-2212-z
52. Zhang Z, Kukita C, Humayun MZ, Saier MH. 2017. Environment-directed activation of the *Escherichia coli flhDC* operon by transposons. Microbiology (Reading) 163:554–569. https://doi.org/10.1099/mic.0.000426
53. van Ditmarsch D, Boyle KE, Sakhtah H, Oyler JE, Nadell CD, Déziel É, Dietrich LEP, Xavier JB. 2013. Convergent evolution of hyperswarming leads to impaired biofilm formation in pathogenic bacteria. Cell Rep 4:697–708. https://doi.org/10.1016/j.celrep.2013.07.026
54. Yang W, Briegel A. 2020. Diversity of bacterial chemosensory arrays. Trends Microbiol 28:68–80. https://doi.org/10.1016/j.tim.2019.08.002
55. Hazelbauer GL, Engström P. 1981. Multiple forms of methyl-accepting chemotaxis proteins distinguished by a factor in addition to multiple methylation. J Bacteriol 145:35–42. https://doi.org/10.1128/jb.145.1.35-42.1981
56. Feng X, Baumgartner JW, Hazelbauer GL. 1997. High- and low-abundance chemoreceptors in *Escherichia coli*: differential activities associated with closely related cytoplasmic domains. J Bacteriol 179:6714–6720. https://doi.org/10.1128/jb.179.21.6714-6720.1997
57. Weerasuriya S, Schneider BM, Manson MD. 1998. Chimeric chemoreceptors in *Escherichia coli*: signaling properties of Tar-Tap and Tap-Tar hybrids. J Bacteriol 180:914–920. https://doi.org/10.1128/JB.180.4.914-920.1998
58. Cannistraro VJ, Glekas GD, Rao CV, Ordal GW. 2011. Cellular stoichiometry of the chemotaxis proteins in *Bacillus subtilis*. J Bacteriol 193:3220–3227. https://doi.org/10.1128/JB.01255-10
59. Zatakia HM, Arapov TD, Meier VM, Scharf BE. 2018. Cellular stoichiometry of methyl-accepting chemotaxis proteins in *Sinorhizobium meliloti*. J Bacteriol 200:e00614-17. https://doi.org/10.1128/JB.00614-17
60. Bray D, Levin MD, Morton-Firth CJ. 1998. Receptor clustering as a cellular mechanism to control sensitivity. Nature 393:85–88. https://doi.org/10.1038/30018
61. Sourjik V. 2004. Receptor clustering and signal processing in *E. coli* chemotaxis. Trends Microbiol 12:569–576. https://doi.org/10.1016/j.tim.2004.10.003
62. Tu Y. 2013. Quantitative modeling of bacterial chemotaxis: signal amplification and accurate adaptation. Annu Rev Biophys 42:337–359. https://doi.org/10.1146/annurev-biophys-083012-130358
63. Parkinson JS, Hazelbauer GL, Falke JJ. 2015. Signaling and sensory adaptation in *Escherichia coli* chemoreceptors: 2015 update. Trends Microbiol 23:257–266. https://doi.org/10.1016/j.tim.2015.03.003
64. Frank V, Piñas GE, Cohen H, Parkinson JS, Vaknin A. 2016. Networked chemoreceptors benefit bacterial chemotaxis performance. MBio 7:e01824-16. https://doi.org/10.1128/mBio.01824-16
65. Sourjik V, Berg HC. 2004. Functional interactions between receptors in bacterial chemotaxis. Nature 428:437–441. https://doi.org/10.1038/nature02406
66. Kalinin Y, Neumann S, Sourjik V, Wu M. 2010. Responses of *Escherichia coli* bacteria to two opposing chemoattractant gradients depend on the chemoreceptor ratio. J Bacteriol 192:1796–1800. https://doi.org/10.1128/JB.01507-09
67. Yang Y, Sourjik V. 2012. Opposite responses by different chemoreceptors set a tunable preference point in *Escherichia coli* pH taxis. Mol Microbiol 86:1482–1489. https://doi.org/10.1111/mmi.12070
68. Hida A, Oku S, Miura M, Matsuda H, Tajima T, Kato J. 2020. Characterization of methyl-accepting chemotaxis proteins (MCPs) for amino acids in plant-growth-promoting rhizobacterium *Pseudomonas protegens* CHA0 and enhancement of amino acid chemotaxis by MCP genes overexpression. Biosci Biotechnol Biochem 84:1948–1957. https://doi.org/10.1080/09168451.2020.1780112
69. Neumann S, Hansen CH, Wingreen NS, Sourjik V. 2010. Differences in signalling by directly and indirectly binding ligands in bacterial chemotaxis. EMBO J 29:3484–3495. https://doi.org/10.1038/emboj.2010.224
70. Li M, Hazelbauer GL. 2004. Cellular stoichiometry of the components of the chemotaxis signaling complex. J Bacteriol 186:3687–3694. https://doi.org/10.1128/JB.186.12.3687-3694.2004
71. Schuster M, Hawkins AC, Harwood CS, Greenberg EP. 2004. The *Pseudomonas aeruginosa* RpoS regulon and its relationship to quorum sensing. Mol Microbiol 51:973–985. https://doi.org/10.1046/j.1365-2958.2003.03886.x
72. Grimm AC, Harwood CS. 1997. Chemotaxis of *Pseudomonas* spp. to the polyaromatic hydrocarbon naphthalene. Appl Environ Microbiol 63:4111–4115. https://doi.org/10.1128/aem.63.10.4111-4115.1997
73. Wu H, Kato J, Kuroda A, Ikeda T, Takiguchi N, Ohtake H. 2000. Identification and characterization of two chemotactic transducers for inorganic phosphate in *Pseudomonas aeruginosa*. J Bacteriol 182:3400–3404. https://doi.org/10.1128/JB.182.12.3400-3404.2000
74. Vangnai AS, Takeuchi K, Oku S, Kataoka N, Nitisakulkan T, Tajima T, Kato J. 2013. Identification of CtpL as a chromosomally encoded chemoreceptor for 4-chloroaniline and catechol in *Pseudomonas aeruginosa* PAO1. Appl Environ Microbiol 79:7241–7248. https://doi.org/10.1128/AEM.02428-13
75. Luu RA, Kootstra JD, Nesteryuk V, Brunton CN, Parales JV, Ditty JL, Parales RE. 2015. Integration of chemotaxis, transport and catabolism in *Pseudomonas putida* and identification of the aromatic acid chemoreceptor PcaY. Mol Microbiol 96:134–147. https://doi.org/10.1111/mmi.12929
76. López-Farfán D, Reyes-Darias JA, Krell T. 2017. The expression of many chemoreceptor genes depends on the cognate chemoeffector as well as on the growth medium and phase. Curr Genet 63:457–470. https://doi.org/10.1007/s00294-016-0646-7
77. Vo L, Avgidis F, Mattingly HH, Edmonds K, Burger I, Balasubramanian R, Shimizu TS, Kazmierczak BI, Emonet T. 2024. Non-genetic adaptation by collective migration. bioRxiv. https://doi.org/10.1101/2024.01.02.573956
78. Fu X, Kato S, Long J, Mattingly HH, He C, Vural DC, Zucker SW, Emonet T. 2018. Spatial self-organization resolves conflicts between individuality and collective migration. Nat Commun 9:2177. https://doi.org/10.1038/s41467-018-04539-4
79. Shao W, Price MN, Deutschbauer AM, Romine MF, Arkin AP. 2014. Conservation of transcription start sites within genes across a bacterial genus. MBio 5:e01398-14. https://doi.org/10.1128/mBio.01398-14
80. Baraquet C, Théraulaz L, Iobbi-Nivol C, Méjean V, Jourlin-Castelli C. 2009. Unexpected chemoreceptors mediate energy taxis towards electron acceptors in *Shewanella oneidensis*. Mol Microbiol 73:278–290. https://doi.org/10.1111/j.1365-2958.2009.06770.x
81. Upadhyay AA, Fleetwood AD, Adebali O, Finn RD, Zhulin IB. 2016. Cache domains that are homologous to, but different from PAS domains comprise the largest superfamily of extracellular sensors in prokaryotes. PLoS Comput Biol 12:e1004862. https://doi.org/10.1371/journal.pcbi.1004862
82. Adler J. 1966. Chemotaxis in bacteria. Science 153:708–716. https://doi.org/10.1126/science.153.3737.708
83. Armstrong JB, Adler J, Dahl MM. 1967. Nonchemotactic mutants of *Escherichia coli*. J Bacteriol 93:390–398. https://doi.org/10.1128/jb.93.1.390-398.1967

84. Croze OA, Ferguson GP, Cates ME, Poon WCK. 2011. Migration of chemotactic bacteria in soft agar: role of gel concentration. Biophys J 101:525–534. https://doi.org/10.1016/j.bpj.2011.06.023
85. Amchin DB, Ott JA, Bhattacharjee T, Datta SS. 2022. Influence of confinement on the spreading of bacterial populations. PLoS Comput Biol 18:e1010063. https://doi.org/10.1371/journal.pcbi.1010063
86. Gescher JS, Cordova CD, Spormann AM. 2008. Dissimilatory iron reduction in *Escherichia coli*: identification of CymA of *Shewanella* oneidensis and NapC of *E. coli* as ferric reductases. Mol Microbiol 68:706–719. https://doi.org/10.1111/j.1365-2958.2008.06183.x
87. Lassak J, Henche A-L, Binnenkade L, Thormann KM. 2010. ArcS, the cognate sensor kinase in an atypical Arc system of *Shewanella oneidensis* MR-1. Appl Environ Microbiol 76:3263–3274. https://doi.org/10.1128/AEM.00512-10
88. Gibson DG, Young L, Chuang R-Y, Venter JC, Hutchison CA, Smith HO. 2009. Enzymatic assembly of DNA molecules up to several hundred kilobases. Nat Methods 6:343–345. https://doi.org/10.1038/nmeth.1318
89. Paulick A, Koerdt A, Lassak J, Huntley S, Wilms I, Narberhaus F, Thormann KM. 2009. Two different stator systems drive a single polar flagellum in *Shewanella oneidensis* MR-1. Mol Microbiol 71:836–850. https://doi.org/10.1111/j.1365-2958.2008.06570.x
90. Levin-Reisman I, Gefen O, Fridman O, Ronin I, Shwa D, Sheftel H, Balaban NQ. 2010. Automated imaging with ScanLag reveals previously undetectable bacterial growth phenotypes. Nat Methods 7:737–739. https://doi.org/10.1038/nmeth.1485
91. Hartmann R, van Teeseling MCF, Thanbichler M, Drescher K. 2020. BacStalk: a comprehensive and interactive image analysis software tool for bacterial cell biology. Mol Microbiol 114:140–150. https://doi.org/10.1111/mmi.14501
92. Colin R, Drescher K, Sourjik V. 2019. Chemotactic behaviour of *Escherichia coli* at high cell density. Nat Commun 10:5329. https://doi.org/10.1038/s41467-019-13179-1
93. Irazoki O, Ter Beek J, Alvarez L, Mateus A, Colin R, Typas A, Savitski MM, Sourjik V, Berntsson RP-A, Cava F. 2023. D-amino acids signal a stress-dependent run-away response in *Vibrio cholerae*. Nat Microbiol 8:1549–1560. https://doi.org/10.1038/s41564-023-01419-6
94. Wilson LG, Martinez VA, Schwarz-Linek J, Tailleur J, Bryant G, Pusey PN, Poon WCK. 2011. Differential dynamic microscopy of bacterial motility. Phys Rev Lett 106:018101. https://doi.org/10.1103/PhysRevLett.106.018101
95. Thornton KL, Butler JK, Davis SJ, Baxter BK, Wilson LG. 2020. Haloarchaea swim slowly for optimal chemotactic efficiency in low nutrient environments. Nat Commun 11:4453. https://doi.org/10.1038/s41467-020-18253-7
96. Findlay RC, Osman M, Spence KA, Kaye PM, Walrad PB, Wilson LG. 2021. High-speed, three-dimensional imaging reveals chemotactic behaviour specific to human-infective *Leishmania* parasites. Elife 10:e65051. https://doi.org/10.7554/eLife.65051
97. Lee S-H, Grier DG. 2007. Holographic microscopy of holographically trapped three-dimensional structures. Opt Express 15:1505. https://doi.org/10.1364/OE.15.001505
98. Wilson L, Zhang R. 2012. 3D localization of weak scatterers in digital holographic microscopy using Rayleigh-Sommerfeld back-propagation. Opt Express 20:16735. https://doi.org/10.1364/OE.20.016735
99. Farthing NE, Findlay RC, Jikeli JF, Walrad PB, Bees MA, Wilson LG. 2017. Simultaneous two-color imaging in digital holographic microscopy. Opt Express 25:28489. https://doi.org/10.1364/OE.25.028489
100. Ershov D, Phan M-S, Pylvänäinen JW, Rigaud SU, Le Blanc L, Charles-Orszag A, Conway JRW, Laine RF, Roy NH, Bonazzi D, Duménil G, Jacquemet G, Tinevez J-Y. 2022. TrackMate 7: integrating state-of-the-art segmentation algorithms into tracking pipelines. Nat Methods 19:829–832. https://doi.org/10.1038/s41592-022-01507-1